THE PENNSYLVANIA STATE UNIVERSITY
SCHREYER HONORS COLLEGE

DEPARTMENT OF PHYSICS

OBSERVATIONS OF IC 443 AT THE HIGHEST ENERGIES USING DATA FROM THE HAWC OBSERVATORY

LEAH HUNT
SPRING 2021

A thesis
submitted in partial fulfillment
of the requirements
for baccalaureate degrees
in Mathematics and Statistics
with honors in Physics

Reviewed and approved* by the following:

Miguel Mostafa
Professor of Physics and Astronomy and Astrophysics
Thesis Supervisor

Richard Robinett
Professor of Physics
Associate Head for Undergraduate and Graduate Students
Honors Adviser

*Electronic Approvals are on file.

Abstract

The supernova remnant IC 443 is a very well studied source in the galactic plane. Many observatories have observed this source with measurements ranging across the electromagnetic spectrum and with energies up to ∼2 TeV. Using data from the HAWC observatory, we further extended these measurements into the multi-TeV range, reaching energies higher than previous measurements. We study the emission region and the source morphology and model the energy spectrum, deriving the physical parameters of the corresponding acceleration mechanisms.

Table of Contents

List of Figures

List of Tables

Acknowledgements

I was supported by the NASA Pennsylvania Space Grant Consortium through the Women in Science and Engineering Research internship program in Spring and Fall 2018. I also received the Undergraduate Research Award from the Office of Science Engagement in the Eberly College of Science at Penn State in Spring 2020. I would like to acknowledge the HAWC collaboration for sharing their data, and reviewing my analyses and presentations.

Chapter 1

Introduction

1.1 Motivation for Analysis

Supernova Remnants (SNRs) are interesting astronomical sources that are produced as a result of a supernova explosion. These initial supernovae are highly energetic, the kinetic energy is generally in the order of 10^{51} erg, and create many of the heavier metals in the universe [1]. Studying the remnants of these explosions is then an area of interest in order to understand their inner workings.

This analysis in particular considers the highest energy emissions in such SNRs, in particular TeV gamma rays. An interesting subset of SNRs to consider when looking for gamma-ray emissions is the group of SNRs interacting with molecular clouds. These SNRs have often been reported producing gamma-ray emissions through the process of pion decay (see Chapter 4 for more detail about pion decay emissions) with examples including W44 and IC 443 [2]. These SNRs are also often interesting in other energy ranges as well, for example in producing interesting properties and forms of emission in X-rays that can be very useful in further studying the SNRs.

One particular such SNR, IC 443, is the primary focus of our analysis. IC 443 is a middle-aged (it is in the 10,000s of years old) core-collapsed SNR located in the galactic plane at a distance of approximately 5,000 light years from Earth [2]. The source has been, and continues to be, extensively studied with observations ranging across the electromagnetic spectrum, discussed in Chapter 2. It is one of the clearest and earliest identified cases of SNRs interacting with molecular clouds and is likewise among the SNRs interacting with molecular clouds that have been identified to produce gamma rays through pion decay [2].

1.2 Data Sources

In order to adequately model the emissions from IC 443, we need data that spans a large portion of the electromagnetic spectrum. While our main focus is on the highest energies and the data from the High Altitude Water Cherenkov (HAWC) observatory, in order to understand these very high energy emissions, we must include emissions from lower energies, especially when fitting physical models as we present in Chapter 4.

1.2.1 HAWC Observatory - Highest Energies

The HAWC observatory is an array of water tanks located near Puebla, Mexico (19° N longitude). HAWC is designed to detect very high energy gamma rays, where very high energy (VHE) is usually defined as greater than 100 GeV. Being a ground detector, HAWC does not detect these gamma rays directly but rather through detecting the particle showers that are created as a result of the gamma rays entering the atmosphere. As the showers reach the water tanks, filled with pure water, the particles in the shower move faster than the speed of light in water, thus producing Cherenkov light that is then detected within the tanks with photomultiplier tubes (PMT). These detections can be used to model the shower, which in turn allows us to reconstruct the arrival direction of the original gamma ray.

It is perhaps unsurprising given the structure described that HAWC collects very large amounts of data. The observatory collects data practically constantly with a duty cycle

over 90% and an instantaneous field of view (FOV) covering approximately 15% of the sky, allowing the observatory to take data from about two-thirds of the sky every day. This large FOV is convenient in that it allows HAWC to view a large number of sources, including many supernova remnants that interact with molecular clouds such as IC 443, W51C, W44, and W41.

Our analysis primarily focuses on HAWC's observations of IC 443 using 5 years of HAWC data. Additional results from and presentation of this dataset can be found in the Third HAWC Catalog [3].

1.2.2 Additional Sources of Data for Additional Energy Ranges

While our main focus is on the highest energies for this analysis, our analysis also requires data from other experiments and other energy ranges. In particular, we also make use of data from each of the following experiments, which are listed in order from highest to lowest energy.

VERITAS

The Very Energetic Radiation Imaging Telescope Array System (VERITAS) is an array of four Cherenkov telescopes which detects gamma rays in the range from the 100s of GeV to a few TeV, an energy range with some overlap to HAWC's energy range. Since VERITAS is a telescope, it can only take data from a small area at a time and particular regions of the sky will only be observed for a limited amount of time. In exchange, however, comes better angular and energy resolutions, though only for point sources or sources with very small extensions. For this analysis, the data from VERITAS ranges from approximately 100 GeV to 2 TeV [4].

Fermi-LAT

Fermi Large Area Telescope (LAT) is a satellite telescope run by NASA. Fermi-LAT detects gamma rays in the MeV to GeV range, with the upper range of energy detection slightly overlapping with that of VERITAS. Being a space telescope, Fermi-LAT is able to directly detect gamma rays since they will be detected before reaching the atmosphere. For this analysis, we use data from Fermi-LAT Pass 8, which is provided for public use [5].

NuSTAR

NuSTAR (Nuclear Spectroscopic Telescope Array) is a pair of space telescopes that measure X-ray data with an energy range in the 10s of keV. The data that we use is publicly available and covers the energy range from $1 - 50$ keV [6].

Clark Lake Radio Observatory

The Clark Lake TPT telescope is a radio telescope run at the Clark Lake Radio Observatory, which uses a system of antennae to detect radio waves. Note that this data is a much lower energy range than the other data we are collecting and will primarily be used to help

bound the higher energy emissions we are interested in. The data that we will use is publicly available and covers the energy range from $0.4 - 210$ μeV [7].

1.3 Objective

While there have been prior studies of IC 443, this work looks to analyze this source at energies above those previously studied, reaching the 10s of TeV. This work looks to show, using data from the HAWC observatory, that IC 443 is indeed TeV bright and to model the emissions in this energy range. Furthermore, we are able to constrain the important physical parameters of the acceleration processes.

Chapter 2

The Region of IC 443

2.1 Prior Observations of the Morphology of IC 443

As it has already been mentioned, IC 443 has been very well studied by a large number of experiments in a wide range of energies. While a description of all such studies would be far beyond the scope of this work, some of the more interesting and relevant components as they pertain to our analysis will be discussed in this section.

2.1.1 Prior X-ray Observations

Though we will generally be focusing on the gamma-ray emissions of IC 443, a brief overview of emissions at lower energy ranges is relevant and interesting enough to warrant some discussion. This source has been studied extensively across many energy ranges, but observations from the X-ray range may be among the more interesting. In general, supernovae interacting with molecular clouds tend to produce a large number of X-rays which can be very useful in analyzing these sources.

In these lower energy ranges, numerous sources are seen in the vicinity of IC 443. For instance, SNR G189.6+3.3 is another supernova remnant viewed in the region. In the X-ray range, even IC 443 itself can be viewed as a set of sub-sources, as was done by Bykov et al [8], with these individual sources potentially explained by different regions of interaction with the molecular cloud, a pulsar wind nebula (PWN) associated with IC 443 or SNR G189.6+3.3, or even other sources in the region.

These complications and additional sources, however, will not be considered for gamma-ray emissions, with the possible exception of SNR G189.6+3.3 which is considered to be possibly associated with Fermi source FGES J0619.6+2229, which is discussed below. For HAWC, the resolution of the detector does not allow for differentiation between the individual components that Bykov et al suggests for the source, and the sources other than IC 443 in the region are assumed to not be emitting gamma radiation. In particular, the emission mechanisms for these energy ranges differ, so we would not necessarily expect the same emissions in both energy ranges. We will, however, see that some emission at the X-ray level can correlate to the emission at the gamma level, in particular synchrotron emission at the X-ray level corresponding to the same sources as potential inverse Compton emission in the gamma range, which will motivate including data from the X-ray range in modelling in Chapter 4.

2.1.2 Prior GeV Energy Observations

FGES J0619.6+2229

In the region of IC 443, Fermi-LAT sees two sources, IC 443, which they also refer to as FGES J0617.2+2235, and a second source FGES J0619.6+2229 [9]. FGES J0619.6+2229 entirely encompases IC 443, with an extension of 0.96° compared to IC 443's 0.34° extension according to Fermi, and FGES J0619.6+2229's energy spectrum is considered to be harder than IC 443's in the Fermi energy range. There is still some uncertainty about what source is associated with FGES J0619.6+2229, though the primary two potential sources suggested by Fermi are SNR G189.6 +3.3, which has been seen emitting at lower energies, or that

FGES J0619.6+2229 is the result of cosmic rays produced by IC 443 that are interacting with the medium nearby the SNR.

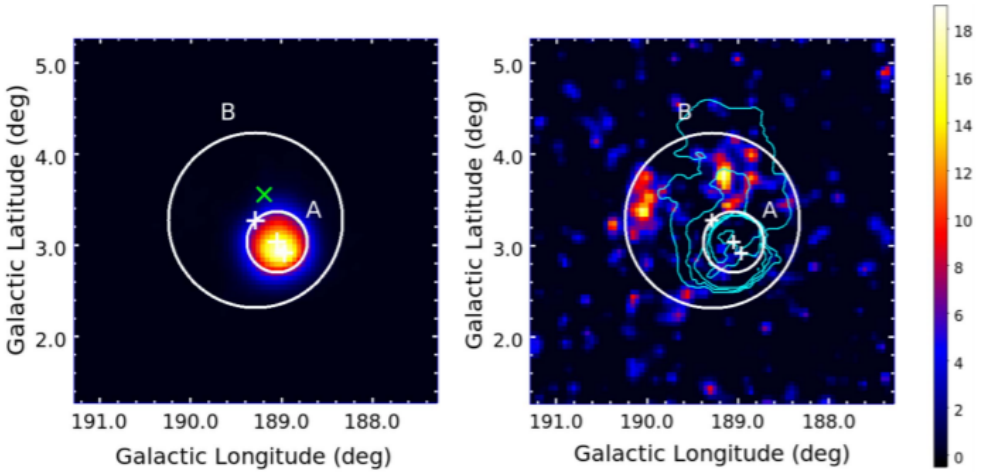

Figure 2.1: This map, taken from Ref. [9], shows the observation of Fermi-LAT of IC 443 and FGES J0619.6+2229. The left shows emission from IC 443, which is notably brighter than that from FGES J0619.6+2229, while the right shows the emission from FGES J0619.6+2229.

In the process of analyzing the source, we considered whether HAWC could too see FGES J0619.6+2229. While we did find IC 443 to be extended in a similar manner to the Fermi-LAT analysis, in fact with a slightly larger extension than Fermi-LAT's 0.34°, there is not sufficient evidence to say that HAWC sees FGES J0619.6+2229, particularly that it sees FGES J0619.6+2229 as a source separate from IC 443 itself.

Spectral Observations from Fermi-LAT

Though not directly pertaining to its morphology, another notable characteristic noticed in this energy range by Fermi-LAT is evidence of pion decay occuring in the source [2]. In particular, the characteristic pion decay "bump," a sudden increase in gamma-ray production, around 200 MeV was observed followed by data consistent with a pion decay spectrum. This is a feature commonly seen in SNRs interacting with molecular clouds and several other experiments have confirmed these observations. There is more discussion on physical models for IC 443 in Chapter 4.

2.1.3 Prior TeV Energy Observations

Observations from VERITAS

Like Fermi-LAT, VERITAS has also observed, and clearly seen, IC 443. These observations show that the energy spectrum appears to extend into the TeV range, and the observations correspond well to data collected by Fermi-LAT. Similar to Fermi-LAT, VERITAS considers the source to be extended over a radius of 0.3°. In addition, Ref. [10] also considers the VERITAS observations in three separate regions, each of radius 0.13°, based on

differences in properties of the source, the three regions being centered around the brightest emission (the right side of the source), a tail coming off of the brightest emission (the left side of the source), and a region with minimal to no molecular cloud interaction (the upper portion of the source, which is notably dimmer than the other two regions). The map in Figure 2.2 can be used as reference for understanding the locations of these regions. We also acknowledge that while the HAWC data was not used to extensively analyze these three regions, the HAWC observations do follow a similar pattern in that the third region contains very few detections while the other two regions behave in a similar manner.

Common Morphology from GeV to TeV Energies

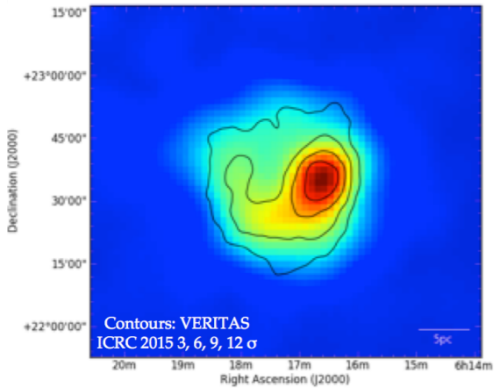

Figure 2.2: This map, taken from Ref. [10], shows data from the Fermi-LAT observatories with overlaying contours from the VERITAS collaboration.

Another notable characteristic of IC 443 is that the source has a common morphology from the GeV to TeV energy range, as noted by observations of Fermi-LAT and VERITAS [10]. A map showing the similarity between the two measurements is shown in Figure 2.2 where the contours from VERITAS's observations and the map from Fermi-LAT clearly agree very well. This indicates that both the TeV and GeV gamma rays are being produced in similar regions of the source, which implies that the gamma rays are likely being produced by similar methods across the two energy ranges. Considering the evidence of pion decay that Fermi-LAT observed, this supports the idea that the TeV gamma rays, or at least those in the energy range seen by VERITAS, would likely also be produced by hadronic methods.[1]

[1]Note that even the physical models presented in Chapter 4 have the pion decay spectrum as dominant up to the energy range observed by VERITAS, in spite of the fact that the fits in Chapter 4 were fit quantitatively without assuming pion decay dominance in either the TeV or GeV range.

2.2 Observations from HAWC

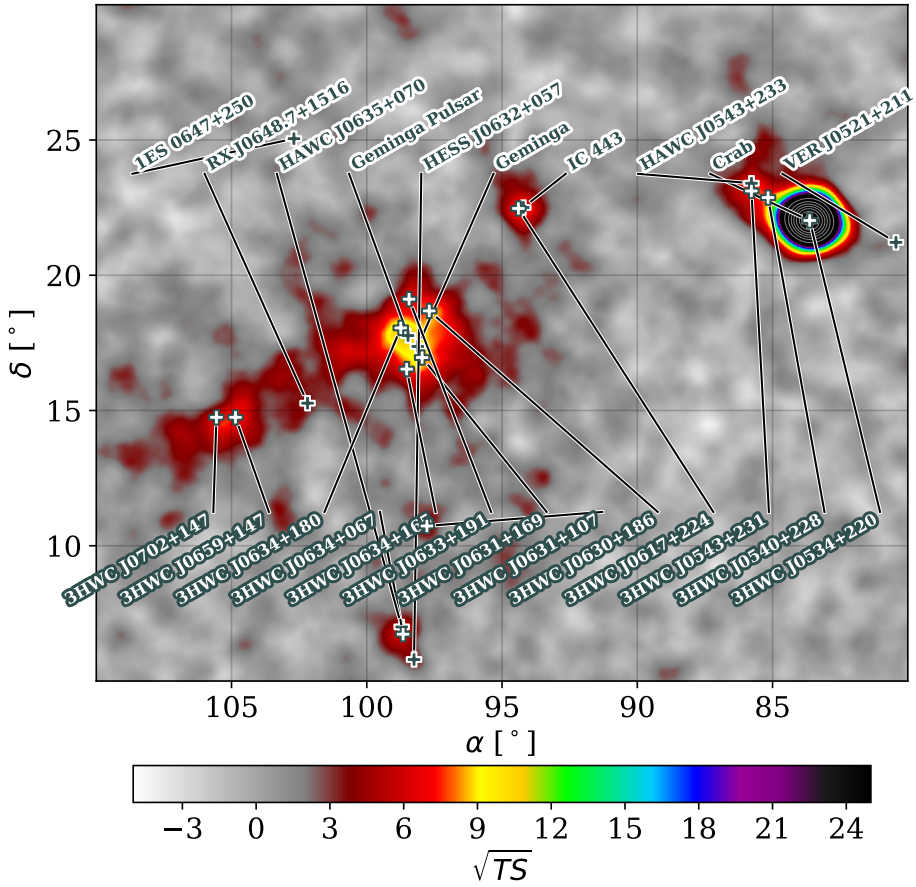

Figure 2.3: This map, taken from Ref. [3], shows the region in which IC 443 is located. Other notable sources in the general region, though not close enough to create complications in modelling the source, include the Crab Nebula (to the right side of the figure) and the Geminga Pulsar (to the left side of the figure). Note that this map does assume a 0.5° extension.

With all of these prior observations as context, we are now interested in viewing IC 443 at the highest energies using the data from HAWC. The general region where IC 443 is located is shown in Figure 2.3. Like with the observations from Fermi-LAT and VERITAS, HAWC likewise considers IC 443 to be an extended source, with the below maps assuming a 0.5° extension on the source. For reference, and to further support our claim that IC 443 is better treated as an extended source, we show both a point source and extended map in Figure 2.4.

While we make a fairly clear case that IC 443 would be well treated as an extended source, we have yet to answer the question of what extension to use. Recall that Fermi-LAT considers the source to be extended at 0.34° and VERITAS sees a very similar extension. As this extension is also reasonable, which we can justify partially from Figure 2.4, for the

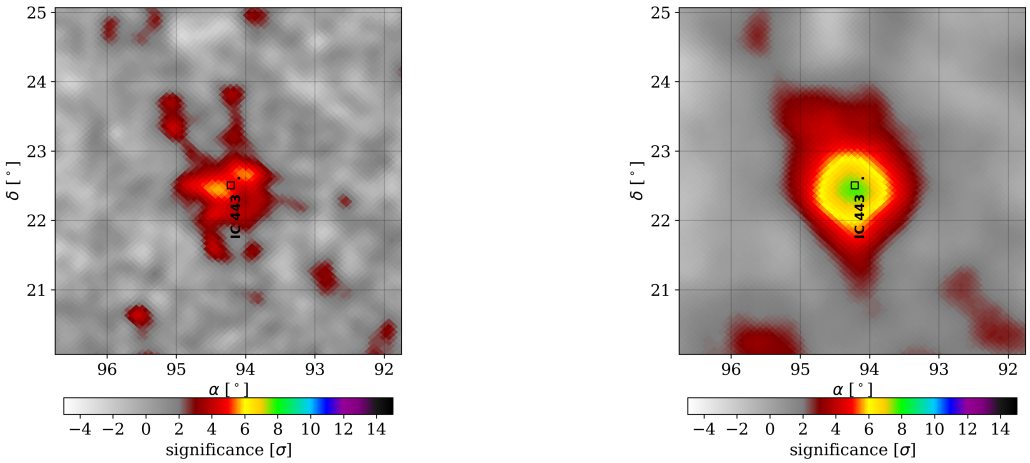

Figure 2.4: These maps show IC 443 as seen by HAWC. The left shows IC443 mapped as a point source while the right shows IC 443 mapped with a .5°extension.

HAWC data, though we do acknowledge that point estimates for the extension under most models were slightly higher than 0.34°. Though, with 0.34° still within the error bands, for consistency we will assume this extension on the source in our next modelling stages unless otherwise stated.

The maximum significance in the extended map occurs at point RA = 94.26 and Declination = 22.43 with a significance of 7.68σ. While this is well over the 5σ threshold that is generally considered for detection, we acknowledge that this is still not an incredibly large number, which does act as a limitation when we further bin the data in energy.

Chapter 3

Empirical Spectrum Modelling for IC 443

A primary goal in our analysis of IC 443 is to model the energy spectrum of the source. The energy spectrum represents the relationship between energy and flux in the observations. Such models can allow us to better understand the emissions of the source and to help us to begin to understand the mechanisms that produced these gamma rays, which will be further explained through physical models in Chapter 4.

3.1 Common Empirical Models

To understand the energy spectrum of IC 443, or many other astrophysical sources for that matter, it is helpful to describe some of the common models used to fit energy spectra. In exploring these models, we should first note that the energy spectra are generally plotted in log scale as these models are usually well represented by power laws.

The first model we will introduce, and one which will be used rather frequently in analysis, is the power law, which in its simplest form represents a line in log scale. As such, it takes two parameters, an index, which represents the slope of the line in log scale, and an amplitude, which is directly related to the constant term for the line.

Similarly, we also may see data fitting a parabola in log scale, a model that is known as a log parabola. Similar to the linear case, the model takes parameters that are analogous to the three constants in the standard form of a parabola equation.

There are also some modifications that are often added to these models. One such common modification is to add a cutoff to the spectrum. This cutoff term causes an exponential, in logspace, decrease in the energy after the cutoff energy, the degree to which it cuts off is determined through the parameter labeled as β, though for the models used in this work we will assume that $\beta = 1$. The model accomplishes this cutoff by introducing a cutoff energy, E_c, and subtracting (in log scale) a power, β, of E divided by the cutoff energy. Of course, this term grows exponentially and is equal to 1 at the cutoff energy, meaning that it will very rapidly grow once $E > E_c$. While a cutoff can be applied to either a power law or log parabola, we will primarily only see the former in the models for IC 443.

Another feature that can be introduced to our models is a break, which is a location in a power law where the index, the slope in log scale, changes. While we will not be using breaks to fit the empirical spectrum of IC 443, they will become more useful in fitting the physical models for the source.

Table 3.1 shows the mathematical models for both the power law and log parabola models as well as showing the application of the cutoff and break for the power law. While for simplicity Table 3.1 does not show a model with both a break and a cutoff, note that a cutoff broken power law is also a potential model and will in fact be utilized in Chapter 4.

We should also acknowledge that in practice, energy is generally scaled by parameter E_0. This energy acts as the reference point for the fit, essentially rescaling energy so that E_0 becomes 1 by dividing energy, the E value in the equations, by E_0.

Model	Equation	Equation as Seen in Log Space
Simple Power Law	$\Phi = A\left(\frac{E}{E_0}\right)^{\alpha}$	$log(\Phi) = \alpha log\left(\frac{E}{E_0}\right) + log(A)$
Cutoff Power Law	$\Phi = A\left(\frac{E}{E_0}\right)^{\alpha} e^{-\left(\frac{E}{E_c}\right)^{\beta}}$	$log(\Phi) = log(A) + \alpha log\left(\frac{E}{E_0}\right) - \left(\frac{E}{E_c}\right)^{\beta}$
Broken Power Law	$\Phi = \begin{cases} A\left(\frac{E}{E_0}\right)^{\alpha_1} & \text{if } \frac{E}{E_0} < \delta \\ \delta^{\alpha_2-\alpha_1}\left(\frac{E}{E_0}\right)^{\alpha_2} & \text{if } \frac{E}{E_0} > \delta \end{cases}$	$log(\Phi) = \begin{cases} \alpha_1 log\left(\frac{E}{E_0}\right) + log(A) & \text{if } \frac{E}{E_0} < \delta \\ \alpha_2 log\left(\frac{E}{E_0}\right) + (\alpha_2-\alpha_1)log(\delta) & \text{if } \frac{E}{E_0} > \delta \end{cases}$
Log Parabola	$\Phi = A\left(\frac{E}{E_0}\right)^{\alpha+\beta log\left(\frac{E}{E_0}\right)}$	$log(\Phi) = log(A) + \alpha log\left(\frac{E}{E_0}\right) + \beta log\left(\frac{E}{E_0}\right)^2$

Table 3.1: Common Models Seen in Fitting Astrophysical Data where Φ represents flux and E represents energy

3.2 HAWC's Energy Spectrum for IC 443

In attempting to understand the highest energy emissions of IC 443, we will begin by fitting the energy spectrum of the HAWC data independently of data from other experiments, focusing solely on the highest energies.

3.2.1 Methods

The fits in this section were done using a software package called LiFF [11]. The fits were done using a likelihood maximization, and we will model the data using a simple power law model. A cutoff power law and log parabola model were also attempted in the fitting process, but we do not have enough data to see a significant improvement in the quality of the fit from these models. See the Appendix for more detail on statistical methods. This model will also assume the extension of the source to be 0.34°.

3.2.2 Model

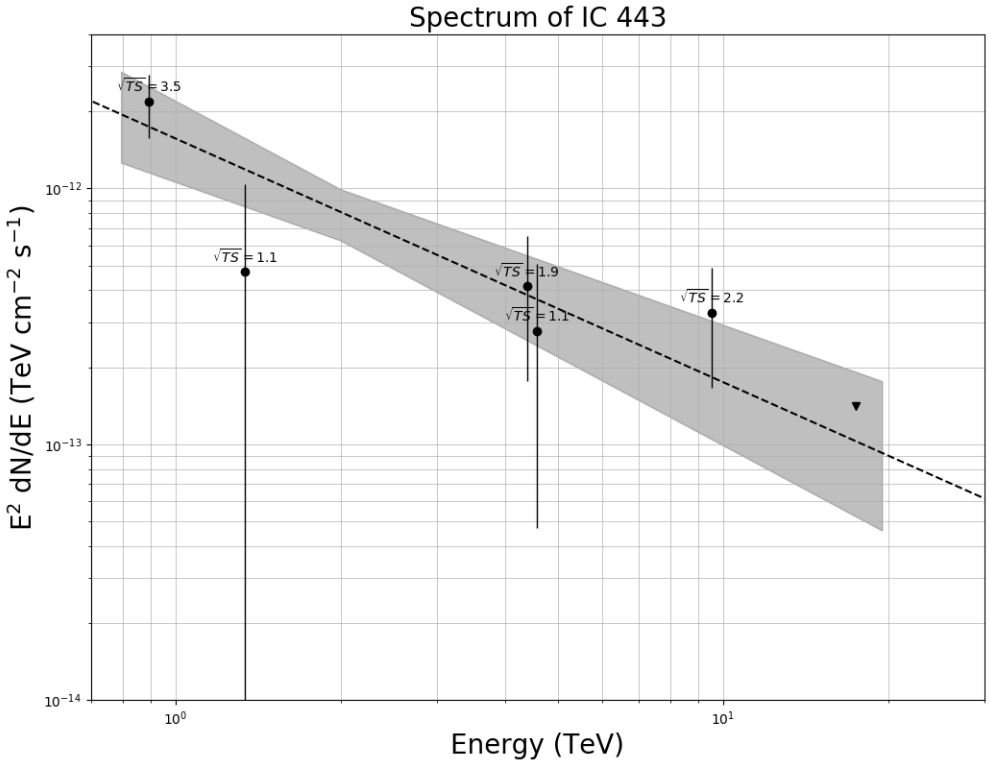

Figure 3.1: This plot shows the energy spectrum of IC 443 using 5 years of data from HAWC.

The resulting fit of the data gives us an index of 3.0 ± 0.2 and a normalization of $(2.0 \pm 0.5) \times 10^{-13}$ TeVcm^{-2}s^{-1} at $E_0 = 2$ TeV. We find that the model shows emissions into the TeV range with an overall TS (test statistic) of 18.

3.3 Joint Fitting a Model for IC 443

3.3.1 Motivation for Joint Fits

While our main goal may be to understand the highest energy emissions of IC 443, understanding a wider range of energy emissions can generally be helpful as well. This wider energy range provides more data that can help us distinguish between patterns that may be nearly indistinguishable on a smaller scale and will also help us to ensure that our data and results remain consistent with other results for the source. These larger patterns will also help us to motivate the choices of physical models to consider in Chapter 4.

3.3.2 Methods

In order to create the joint fit, we will be using the python package ThreeML [12]. ThreeML uses a maximum log likelihood, a process described in more detail in the Appendix,

to fit data from various sources (i.e. in different formats) through plugins that can be used to either input flux points or to input data specific to particular experiments. It uses a likelihood function to locate the global minimum [12]. The high energy gamma-ray data that we fit through ThreeML is the data from HAWC, VERITAS, and Fermi-LAT.

3.3.3 Joint Model

In fitting the joint spectrum, we found that a log parabola model better fit the data. Looking at the data points in Figure 3.2, the motivation for such a model is fairly clear as we do see a curved pattern to the data, particularly in the lowest energies of the Fermi-LAT data. The resulting fit parameters give us a model with parameters $A = 1.05 \pm .06 \times 10^{-12}$ $(\text{cm}^2\text{TeVs})^{-1}$ at $\text{E}_0 = 2$ TeV, $\alpha = -2.94 \pm .04$, and $\beta = .05 \pm .04$.

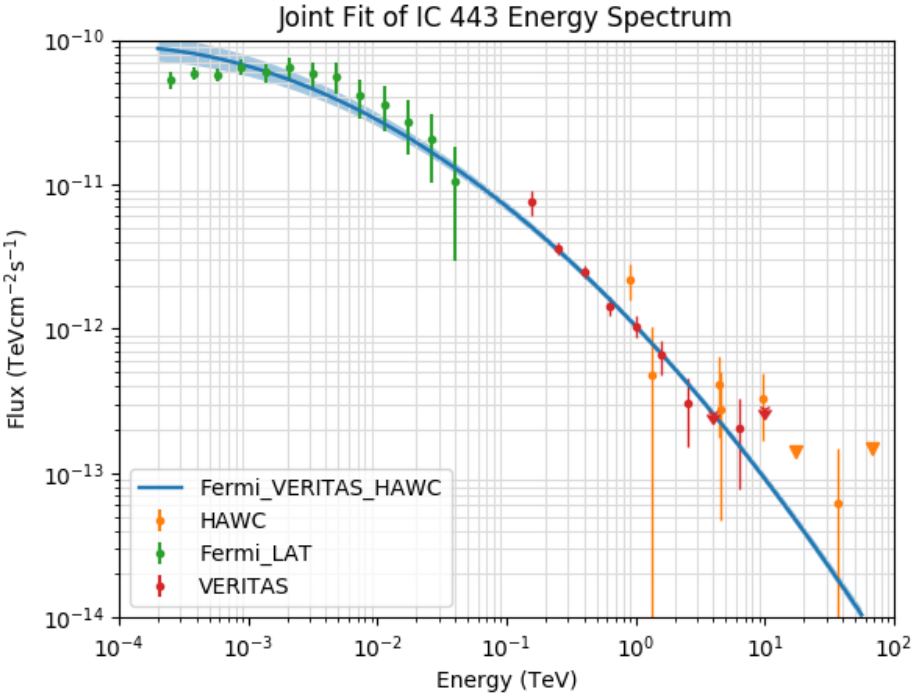

Figure 3.2: This plot shows the joint fit of IC 443. The green points come from Ref. [5], the red points come from Ref. [4], and the yellow points show the flux points from Figure 3.1.

Figure 3.2 also motivates some aspects of physical modelling. For instance, the curved feature in the Fermi-LAT data occurs in the 100s of MeV, and could be considered characteristic of a pion decay spectrum, which is said to initialize with such a bump then follow an empirical model.[1] While it is clear that a simple power law would fit each experiment individually, a power law cannot fit across the whole energy range. Considering these characteristics of the spectrum, our observations foreshadow the results we will find in Chapter 4 as we construct these physical models.

[1]The empirical model which it follows is approximately the distribution of protons at the source. The process of pion decay and the resulting models will be discussed in more detail in Chapter 4.

Chapter 4

Physical Model of IC 443

4.1 Model Structure

Beyond the empirical models that show the general shape of emissions, we want to explore physical models that explain the source of these observed gamma rays.

One common source of gamma rays, particularly in supernova remnants interacting with molecular clouds, is the hadronic mechanism of pion decay. Emission from pion decay occurs when a neutral pion, generally created in a collision between two protons, decays into two gamma rays, a process that generally happens relatively soon after the formation of the pion [13]. Detection of emission due to pion decay appears as a "pion-decay bump" around 200 MeV in the energy spectrum where the spectrum rises up to about 200 MeV before taking approximately the shape of the distribution of protons at the source at higher energies. This characteristic feature has been identified in IC 443 by data collected from Fermi-LAT, who identify pion decay to be the primary source of gamma-ray emissions [2].

We can also consider leptonic emission through inverse Compton scattering, another common method of gamma-ray production. Inverse Compton scattering is a process by which electrons collide with photons. This collision transfers energy from the electron to the photon, thus creating gamma rays [14]. This model provides an alternative model by which the measured gamma rays could have been produced, and we will consider both this mechanism and pion decay models in attempting to explain the gamma-ray production.

In order to properly bound the inverse Compton emissions, we should also consider synchrotron emissions. Synchrotron emission is generated by charged particles, in this case electrons, moving quickly through magnetic fields [15]. Synchrotron emission occurs at lower energies than the gamma emissions that we are primarily interested in with the emissions not exceeding the X-ray spectrum. However, since this emission is generated from the same electrons as the inverse Compton emission, in addition to a dependence on the magnetic field at the source.

Our model will consider the total emissions of the source to be the sum of the emissions produced by these three methods: pion decay, inverse Compton, and synchrotron emissions. The free parameters of the model will be the parameters of the distribution of the protons, the parameters of the distribution of the electrons, and the magnetic field at the source, the first applying to the component of the emission from pion decay, the second applying to the component of the emission from inverse Compton, and the last two applying to the component of the emission from syncrotron.

4.2 Fitting Methods

In order to fit this model, we use the python package naima [16]. Naima contains built-in physical models for each of our three acceleration mechanisms and will allow us to fit our total model to data referenced in Chapter 1, ranging from radio to gamma-ray energies. Naima's fitting algorithm uses the package emcee in order to employ a Metropolis-Hastings Markov Chain Monte Carlo (MCMC) sampler with an affine invariant, a method that is described in more detail in the Appendix.

Electron Model	Proton Model	BIC	ML
Broken Cutoff Power Law	Broken Cutoff Power Law	126.7	-40.8
Broken Power Law	Broken Cutoff Power Law	124	-41.5
Broken Power Law	Broken Power Law	142.2	-52.7
Broken Power Law	Cutoff Power Law	121.6	-44.4

Table 4.1: This table shows the BIC and log likelihood values for each of the models discussed.

4.3 Model Selection

4.3.1 Initial Model

For our model, we will start by considering the most general case for a power law spectrum for the proton and electron spectra: a broken cutoff power law. Our results give parameter estimates of $A = 4.8 \times 10^{48}$/TeV at $E_0 = 1$ TeV, $\alpha_1 = 2.7$, $\alpha_2 = .9$, $E_{cut} = 5.3$TeV, and $E_{break} = 4.1$ TeV for the proton spectrum and $A = 1.1 \times 10^{47}$/TeV at $E_0 = 10$ TeV, $\alpha_1 = 1.5$, $\alpha_2 = 3.6$, $E_{cut} = 1302$ TeV, and $E_{break} = .05$ TeV for the electron spectrum with a magnetic field of 13μG. This model, however, is only the first that we will attempt as we look to find a simpler model to explain the data. In particular, we will attempt to remove the break and/or cutoff from the proton and/or electron spectra then compare the models to see which are better.

To compare different models, we will use maximum log likelihood and the Bayesian Inference Criterion (BIC). Note that a better model will have a higher log likelihood but lower BIC. More information on these two criteria and methods for model selection can be found in the Appendix. Though each of the proposed models and the model selection process are discussed in more detail in the following sections, the results for each of these proposed models is shown in Table 4.1.

4.3.2 Removing the Cutoff from the Electron Distribution

The first, and perhaps most obvious, simplification we can make to our model is to notice that the current fit has its energy cutoff for the electron distribution above 1000 TeV, which is far above the energies that we are considering. This implies that the cutoff is unnecessary in the fit. Looking at Table 4.1, we see that the results support this conclusion, and thus, we will proceed with the assumption that the electron distribution follows a broken power law.

4.3.3 Submodels for the Proton Spectrum

We can also consider submodels for the proton spectrum. We will consider three possible models for the proton distribution: a broken power law, a cutoff power law, and a broken cutoff power law, the latter being the current model.

In considering the three models, it is clear that the broken power law model is the weakest of the three, having a much worse value for both criteria. The remaining two models,

however, both seem to fit the data fairly well. While the broken cutoff power law has a better log likelihood, the cutoff power law holds a slight advantage in BIC, thus indicating that the improvement brought by the break may not sufficiently compensate for the added complexity brought by the break. However, seeing as these models are fairly close (the odds ratio between the two is only approximately 3.4), we will continue to consider both of these models.

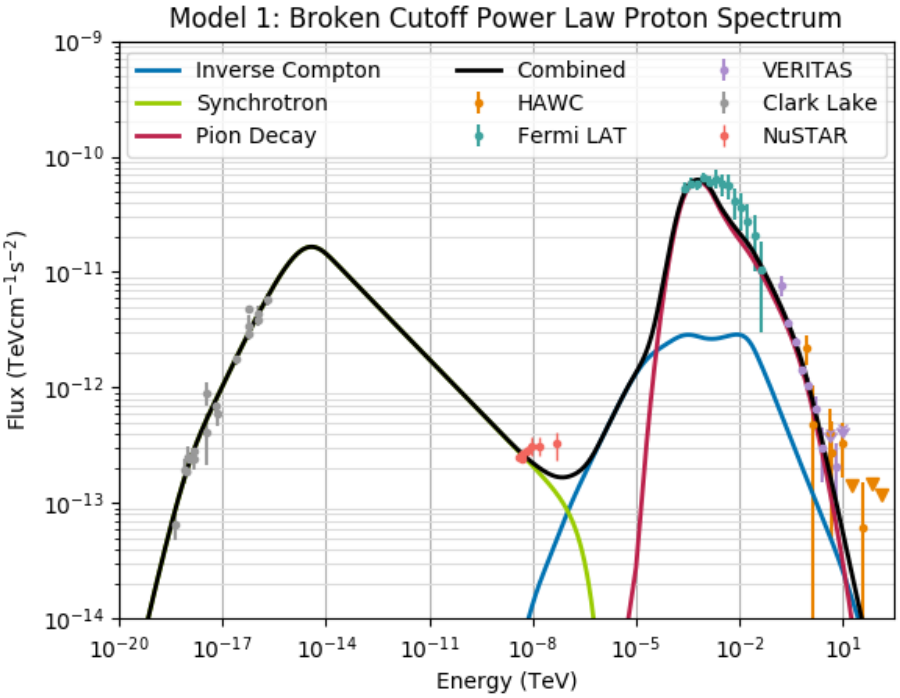

Figure 4.1: This plot shows the results of the model assuming a broken cutoff power law for the proton spectrum and broken power law electron spectrum.

			Model 1			Model 2		
	Parameter	Unit	Value	-Err	+Err	Value	-Err	+Err
	Magnetic Field	μG	13.5	2.1	1.4	14.4	1.6	1.0
Electron	log(Amplitude)	1/TeV	46.25	.31	.35	46.20	.4	.24
	α_1	-	1.74	.11	.07	1.76	.07	.09
	α_2	-	3.61	.07	.12	3.48	.07	.13
	log(break)	TeV	-1.25	.15	.21	-1.51	.15	.21
Proton	log(Amplitude)	1/TeV	48.81	4.4	.08	49.14	.11	.05
	α_1	-	2.60	.06	.03	2.45	.03	.03
	α_2	-	3.33	.24	.44	-	-	-
	log(break)	TeV	.46	.11	.06	-	-	-
	log(cutoff)	TeV	1.91	.26	.36	.42	.03	.05

Table 4.2: This table shows the model parameters for the two chosen models where model 1 represents the model with a broken cutoff power law proton spectrum and model 2 represents the model with a cutoff power law proton spectrum. Thus, for model 2, there is only one spectral index, α_1.

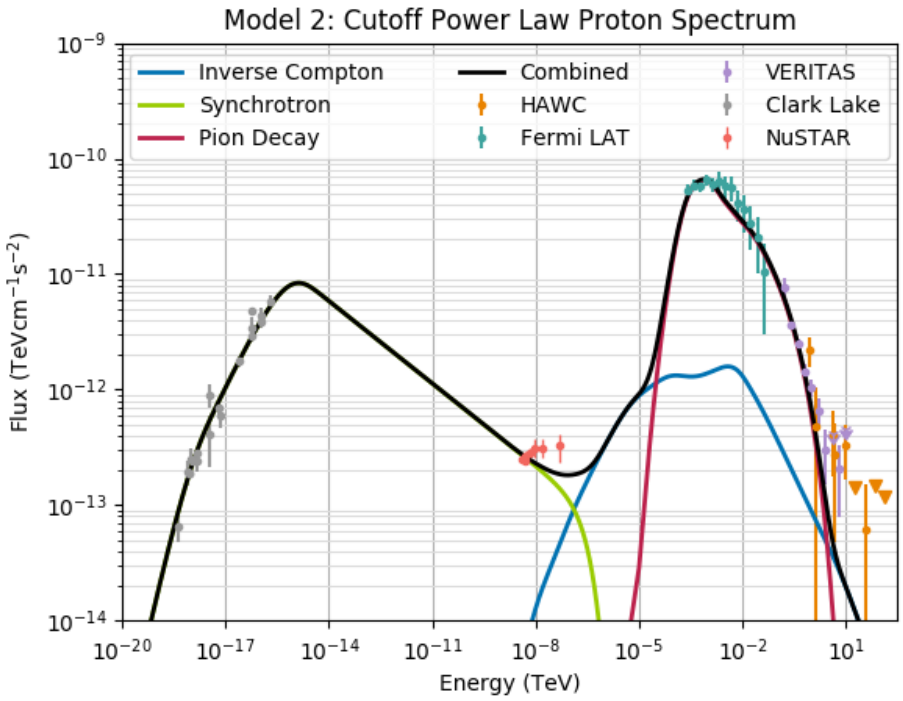

Figure 4.2: This plot shows the results of the model assuming a cutoff power law for the proton spectrum and broken power law electron spectrum.

4.4 Further Comparison of Selected Models

In the model selection phase, we found two models that seemed to be reasonable fits for our data based primarily on the criterion of BIC. We will now consider these models further.

4.4.1 Comparing the Models at the Highest Energies

Recall that the main purpose of developing these models was to understand the high energy emissions of IC 443. Thus, it is reasonable that we pay particular attention to the implications of both of these models at the highest energies as well as analyzing how well they fit the HAWC data.

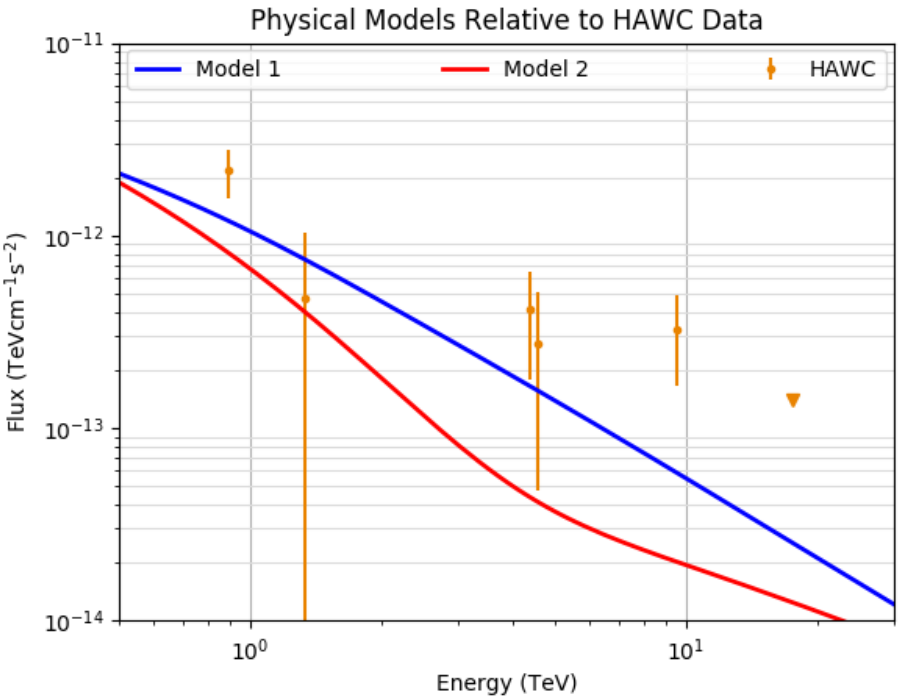

Figure 4.3: This plot shows the same models as Figure 4.1 and Figure 4.2 zoomed in to the highest energies. Recall that Model 1 refers to the model with a broken cutoff power law proton spectrum while Model 2 refers to the model with a cutoff power law proton spectrum. Notice how the quality of the fit at these energies varies between the models.

When considering only the highest energies, the broken cutoff power law model for the proton spectrum produces a better overall fit compared to the cutoff power law model, which seems to create a fit that consistently predicts a lower flux than the data. This difference is in contrast to the overall fit results, where the two models were comparable. This also provides further evidence toward the use of the more complex model, in spite of its slightly lower BIC when considering the total fit.

4.4.2 Commonalities Between Models

In understanding our two potential models, with particular focus on the distribution of protons at the source, we also want to consider what common features our two models share. First, we note that the spectrum of electrons in each model is rather similar with the fitted values for each parameter, including the magnetic field, being within uncertainties between the two models.

The proton distributions, however, are quite different. While parameters like the normalization and spectral index, considered the pre-break spectral index for the broken power law with cutoff, are significantly different, their differences falling outside of statistical errors, we do see some similarity in the two models. In particular, we see that the spectrum does feature some hardening around the same location in both models, in the range between 2.5 and 3 TeV. The cutoff power law spectrum accounts for this hardening by applying the cutoff while the latter model applies it through a break with a second larger index. Thus, there does appear to be some feature in the spectrum around this energy that both models attempt to account for.

We then consider where the cutoff for the broken cutoff power law is applied, as this cutoff is the primary spectral feature excluded from the other model. The cutoff occurs at an energy of approximately 80 TeV. The presence of such a feature in this energy range may help explain why this model seems to fit the highest energy better as the information that the additional complexity is adding is targetted almost entirely to the range of the HAWC data.

4.5 Implications of Selected Models

Looking at our results, we see that the results are consistent with prior reports from Fermi-LAT. Our model indeed shows pion decay as the dominant emission mechanism in the GeV energy range, and even partially into the TeV range. Likewise, the results of the fit are comparable to the parameters derived in Ref. [2]. We do, however, also acknowledge an additional inverse Compton component that then becomes dominant, though with a rather low flux, above approximately 10 TeV in both of our models.

We can also consider the model fit at the lower energies, especially in acknowledging that our fit spans approximately 20 orders of magnitude in energy across the electromagnetic spectrum. Though our synchrotron fits do not appear to fully explain the X-ray emissions, our fits are similar to those produced in Ref. [6], the source for the X-ray data. This result is actually expected as synchrotron emission is not the sole producer of X-rays, as we discussed in Chapter 2, and in fact Ref. [6] concludes that synchrotron emission is not a major producer of X-rays for IC 443. Since we are predominantly focusing on the highest energy emissions, creating a better fit for this energy range through additional modelling is unnecessary.

Furthermore, we can use our models to derive energetics for the source. Integrating over the proton spectra, we get $(9\pm1)\times10^{50}$ erg, and for the electron spectrum we get $(2\pm1)\times10^{48}$ erg. These results are consistent between both of our chosen models. The result that the proton energy is much higher than that of the electrons should not be surprising considering

that the main emission at higher energies was shown to be pion decay. Putting this in the context of total energy in the source, the in initial supernova can release in the range of 10^{51} erg, we can see that our proton spectrum in particular appears to account for a fair amount of this energy.

Chapter 5

Discussion and Conclusion

5.1 Summary of Results

Our primary results were to analyze the gamma-ray emissions of the SNR IC 443 at the highest energies, extending to energies beyond those previously observed. We began by observing the significance maps of the source using HAWC data, confirming the observations and relating observations to the numerous observations made previously. We then analyzed the spectrum of the source, establishing the spectrum in the TeV range, and then we combined these observations with data from other experiments to create a more comprehensive fit to motivate physical models for the source.

This led to our primary result: a physical model of the source to explain the emission mechanisms. We found that our model remained consistent with prior studies, identifying pion decay to be the primary source for gamma rays in the TeV range, though we were able to add an inverse Compton component which appears to be the primary source of emission below 10 TeV.

5.2 Assumptions and Limitations

Over the course of analysis, we should also acknowledge the limitations of our results. For one, we acknowledge that the time periods in which data was taken were slightly different between experiments. Though we do not expect this to have a large influence on the analysis, it could still be a slight source of variation between the measurements.

As we have noted several times in analysis, we are also limited by the angular resolution of the detector itself. As such, we assumed that the emission was consistent across the source, which is not necessarily a fully accurate assumption, for example based on the analysis of VERITAS which shows slightly different emissions in the different regions of the source. We likewise make some assumptions about the source extension, generally considering it to be equivalent to the extension measured by Fermi-LAT in order to maintain consistency and based on the fact that the estimated extension from HAWC is approximately also equal to $0.34°$. This set of assumptions limits the scope of our study, considering only the remnant as a whole instead of considering the different regions of the remnant individually.

We should also comment on the decision of where IC 443 is located. There are slight variations between experiments as to where IC 443 is considered to be located, which is generally measured by the point of maximum significance for the source. We find, however, that, particularly when the extension is taken into account, the differences between these locations is generally small. In fact, comparing the locations used by Fermi-LAT, HAWC, and VERITAS, the distances between the locations is less than $0.2°$, which is well within the 68% containment of HAWC's point spread function (PSF) [17]. Likewise, difference in location could happen for multiple reasons, both based on the detectors themselves or based on the actual emissions of the remnant. Since we are considering the remnant as a whole, these slight differences in location do not represent an issue for our study because we are integrating over the whole region.

Furthermore, we also acknowledge the limits of the amount of data that we have for this analysis. While in HAWC's observations IC 443 does surpass the 5σ significance threshold, the total significance is still no more than 8σ over the whole energy range. As the detector

continues to take data and as new detections of these very high energy gamma-rays emerge, we can of course expect to gain improved models.

5.3 Suggestions for Further Study

In considering study beyond this analysis, we should recall that IC 443 is but one example of a SNR within HAWC's field of view. There are many other such SNRs, many of which interact with molecular clouds, which could be examined through analysis similar to that conducted here in order to provide additional evidence and data as to the general behavior of such sources. Such efforts have been undertaken, such as in [1], which demonstrates HAWC's observations for multiple SNRs. Furthermore, sources such as Fermi-LAT's SNR catalog [9] can provide additional inspiration to the search for SNRs emitting at the highest energies and their subsequent analysis. Of course, as more data becomes available, these potential sources, and even sources like IC 443 which have already been analyzed, should continue to be monitored as increased amount of data can allow for improved measurements and precision.

Bibliography

[1] Henrike Fleischhack. A Survey of TeV emission from Galactic Supernova Remnants with HAWC, 2019.

[2] M. Ackermann, M. Ajello, A. Allafort, L. Baldini, J. Ballet, G. Barbiellini, M. G. Baring, D. Bastieri, K. Bechtol, R. Bellazzini, and et al. Detection of the Characteristic Pion-Decay Signature in Supernova Remnants. Science, 339(6121):807–811, Feb 2013.

[3] A. Albert, R. Alfaro, C. Alvarez, J. R. Angeles Camacho, J. C. Arteaga-Velazquez, K. P. Arunbabu, D. Avila Rojas, H. A. Ayala Solares, V. Baghmanyan, E. Belmont-Moreno, and et al. 3HWC: The Third HAWC Catalog of Very-high-energy Gamma-Ray Sources. The Astrophysical Journal, 905(1):76, Dec 2020.

[4] Sajan Kumar. private correspondence.

[5] A. A. Abdo, M. Ackermann, M. Ajello, L. Baldini, J. Ballet, G. Barbiellini, D. Bastieri, B. M. Baughman, K. Bechtol, R. Bellazzini, and et al. Observation of Supernova Remnant IC 443 with the Fermi Large Area Telescope. The Astrophysical Journal, 712(1):459–468, Mar 2010.

[6] Shuo Zhang, Xiaping Tang, Xiao Zhang, Lei Sun, Eric V. Gotthelf, Zhi-Yu Zhang, Hui Li, Allen Cheng, Dheeraj Pasham, Frederick K. Baganoff, Kerstin Perez, Charles J. Hailey, and Kaya Mori. NuSTAR Detection of a Hard X-Ray Source in the Supernova Remnant-molecular Cloud Interaction Site of IC 443. ApJ, 859(2):141, June 2018.

[7] W. C. Erickson and M. J. Mahoney. Clark Lake observations of IC 443 and Puppis A. ApJ, 290:596–601, March 1985.

[8] A. M. Bykov, A. M. Krassilchtchikov, Yu. A. Uvarov, H. Bloemen, F. Bocchino, G. M. Dubner, E. B. Giacani, and G. G. Pavlov. Isolated X-Ray–Infrared Sources in the Region of Interaction of the Supernova Remnant IC 443 with a Molecular Cloud. The Astrophysical Journal, 676(2):1050–1063, apr 2008.

[9] M. Ackermann, M. Ajello, L. Baldini, J. Ballet, G. Barbiellini, D. Bastieri, R. Bellazzini, E. Bissaldi, E. D. Bloom, R. Bonino, and et al. Search for Extended Sources in the Galactic Plane Using Six Years of Fermi-Large Area Telescope Pass 8 Data above 10 GeV. The Astrophysical Journal, 843(2):139, Jul 2017.

[10] B. Humensky and VERITAS Collaboration. The TeV Morphology of the Interacting Supernova Remnant IC 443. In 34th International Cosmic Ray Conference (ICRC2015), volume 34 of International Cosmic Ray Conference, page 875, July 2015.

[11] HAWC Collaboration. Aerie (version 2.02.00), 2015.

[12] G. Vianello, R. J. Lauer, J. M. Burgess, H. Ayala, H. Fleischhack, P. Harding, M. Hui, S. Marinelli, V. Savchenko, and H. Zhou. The Multi-Mission Maximum Likelihood framework (3ML). In Proceedings of the 7th International Fermi Symposium, page 130, October 2017.

[13] Ervin Kafexhiu, Felix Aharonian, Andrew M. Taylor, and Gabriela S. Vila. Parametrization of gamma-ray production cross sections for p p interactions in a broad proton energy range from the kinematic threshold to PeV energies. Phys. Rev. D, 90(12):123014, December 2014.

[14] D. Khangulyan, F. A. Aharonian, and S. R. Kelner. Simple Analytical Approximations for Treatment of Inverse Compton Scattering of Relativistic Electrons in the Blackbody Radiation Field. ApJ, 783(2):100, March 2014.

[15] F. A. Aharonian, S. R. Kelner, and A. Yu. Prosekin. Angular, spectral, and time distributions of highest energy protons and associated secondary gamma rays and neutrinos propagating through extragalactic magnetic and radiation fields. Physical Review D, 82(4), Aug 2010.

[16] V. Zabalza. Naima: a Python package for inference of particle distribution properties from nonthermal spectra. In 34th International Cosmic Ray Conference (ICRC2015), volume 34 of International Cosmic Ray Conference, page 922, July 2015.

[17] A. U. Abeysekara, A. Albert, R. Alfaro, C. Alvarez, J. D. Alvarez, R. Arceo, J. C. Arteaga-Velazquez, H. A. Ayala Solares, A. S. Barber, B. Baughman, and et al. The 2HWC HAWC Observatory Gamma-Ray Catalog. The Astrophysical Journal, 843(1):40, Jun 2017.

[18] Daniel Foreman-Mackey, David W. Hogg, Dustin Lang, and Jonathan Goodman. emcee: The MCMC Hammer. Publications of the Astronomical Society of the Pacific, 125(925):306–312, Mar 2013.

Appendix

Throughout this analysis, we use a vast number of statistical methods in order to fit our data to various models. This appendix is meant to provide more light on these methods and better explain the statistics behind the fitting algorithms used.

Frequentist vs Bayesian Statistics

Within our analysis, we see methods applying both frequentist and bayesian methods. While an analysis of all aspects of the debate and uses of these two ideologies in statistics would be excessive for our purposes, a basic understanding of the differences between the two will still be useful in understanding the methods.

Frequentist Statistics

Of the two, the frequentist ideology is generally the better known and more commonly taught in introductory statistics. This method considers the probability of an event to be a long run average, and it considers the truth to be set in stone. Therefore, if we were to attempt to determine if event A happened, we may say that, if many samples were taken, in 10% of such scenarios we would have event A, but the probability that event A happened this time is set to either 0 or 1; it either did happen or it did not happen. Likewise, x% confidence intervals would be interpreted as a range of values for which the produced estimate will fall in for x% of repetitions of the experiment. The confidence interval actually has no bearing on the estimate we produced (and to say that there is an x% chance that the true value falls in the range of the confidence interval is entirely wrong as we consider the true value to be fixed).

Bayesian Statistics

Bayesian statistics takes a slightly different approach to probability. In this approach, we consider probability to be be a degree of belief that something is true. Unlike in the frequentist method, we can make statements such as that we are x% confident that the true value lies in some confidence interval or that we are x% confident that event A happened.

The basis of Bayesian statistics is Bayes Theorem and conditional probability ($p(A|B) = \frac{p(A)p(B|A)}{p(B)}$) as this approach considers all probabilities as conditional on some prior knowledge. This prior knowledge, i.e. the prior, is set by the statistician and represents anything that is

already known about the value. For example, you may know that the parameter should be positive or that it should be normally distributed around 0. For scenarios where you don't have particular information to input, you would use something called an uninformative prior.[1]

The Bayesian and Frequentist Debate

Which version of probability is better is a debatable topic. A frequentist would argue that Bayesian statistics inherently biases results by relying on the prior, something that the statistician decides. On the other hand, a Bayesian would argue that a frequentist calculates a value that is not inherently useful and that is prone to misinterpretation, something that the frequentist would likely disregard as a fault of the user, not the method. The Bayesian would argue that the Bayesian method produces values based on what the user actually cares about: a degree of certainty based on pre-existing information.

In reading this short explanation, do not be confused into thinking that the statistical world is comprised of only Bayesians and frequentists. Most statisticians will use aspects of both as both methods are valid with which is considered better often changing by scenario. Even in this work we apply both aspects of Bayesian and frequentist methodologies in the various stages of analysis, basing our decisions largely on available software and remaining consistent with common methods used in the field. Thus, the real take away is that while these two methods are different and need to be interpreted differently, they are both valid and hold a place in the statistical world.

Method of Maximum Likelihood and Regression

The basic premise of the method of maximum likelihood is to calculate a value called a likelihood and maximize it over your parameters. The likelihood function L represents a probability distribution such that we want to maximize $L(X|\theta) = \prod_{i=1}^{n} L(X|\theta)$ where θ represents the model parameters. In practice, we generally consider the natural log of the likelihood function primarily because it simplifies calculations and can prevent underflow (in practice, $L(X|\theta)$ is generally a very small number). This transformation is valid because it preserves order (if $x < y$ then $ln(x) < ln(y)$), we are dealing with probabilities that will always be greater than 0, and we only care about the value of the likelihood in a relative sense, i.e. we want to maximize the value and can compare the values of the likelihood between different models, but the numerical value of the likelihood itself carries little to no meaning. We can then differentiate the function with respect to each of our parameters, set each derivative to 0, and proceed to identify the maximum.

Though this is the proper statistical method for likelihood maximization, in reality, most fitting algorithms, including those we use, will use numerical methods to find the maximum as opposed to the calculus approach that a statistician would do by hand. Though there

[1] The premise of an uninformative prior is somewhat debated. While it doesn't explicitly provide information to the fit, even an uninformative prior still inadvertently includes some information. There is likewise much debate on what should be used as an uninformative prior, though for the sake of this discussion, it is reasonable to think of an uninformative prior as essentially a flat line (in other words, that the parameter is a number and that we put no more probability on any one number than any other).

are many such algorithms, which are generally considered minimization algorithms instead of maximization algorithms since minimizing $-f$ is the same as maximizing f, most rely on some form of guessing one or more starting points then attempting to minimize from that location in methods such as gradient descent, a method where the point "moves" in the direction in which the function is decreasing at the greatest rate.

In the course of this discussion, we should also mention the role of regression in our analysis. Considering the models that we introduced in Chapter 3, it shouldn't be surprising to realize that we could also estimate our parameters using regression techniques. In fact, we would find that, if we use a model with a normally distributed error term, these regression methods would reach the same result as our above approach. However, we will exclude further discussion of such methods considering that, especially based on the amount and type of data being fitted, the algorithms applied for fitting our data in the empirical models far favored the methods discussed in the above paragraphs.

Markov Chain Monte Carlo

For our physical models, we use the Bayesian method of Markov Chain Monte Carlo (MCMC). It is worth recalling that the functions fit for these models were very complex, which would make the techniques discussed in the previous section more difficult to implement.

The premise of Markov Chain Monte Carlo methods can really be found in their name. The method constructs a Markov Chain whose long run distribution match the intended distribution, which for our case refers to the distribution that best matches[2] the data and uses said chain in order to create a Monte Carlo sample of the desired distribution which will allow us to create parameter estimates and confidence intervals.

Metropolis-Hastings

There are several forms of MCMC methods, though the one that is used by emcee, the underlying sampler for naima, is Metropolis Hastings. The construction of the chain works as follows. From the current state (i.e. parameter value or values) we randomly propose a new state, chosen by some probability distribution, which we can choose; we will call our choice S. We will then choose whether to accept or reject this step. Let $p(x|D)$ represent the likelihood function of x given the observed data. Then the probability of transitioning betwen states is $min\left(1, \frac{p(x_2|D)S(x_1|x_2)}{p(x_1|D)S(x_2|x_1)}\right)$. [18] Loosely speaking, if our proposed move is better, then we go there and if it is worse, we go there with some probability that depends on how much worse the new location is. While it may seem unintuitive to allow for movement in a direction that gets worse, the purpose of allowing such a move is to help the chain to move out of local maxima in an effort to help it find global maxima. It should also be rather

[2]As a disclaimer, though efforts are made to improve the chances of arriving at the global maximum, it is still possible for the fit to converge to a local optimum. In fact, as a general rule, optimization algorithms cannot guarantee that they will locate a global maximum in general cases, though of course in cases like concave functions which have only one local or global maximum, these algorithms can find the global maximum.

intuitive to see that this chain should approach a (hopefully global) maximum in the long run.

In order to get our samples in order to get our parameter estimate, we then want to sample from the long run distribution. In order to do so, we must first allow a certain amount of burn in steps, which allows the chain to move from the initial position to the long run, then once the chain has stabilized take our samples. Note that the number of burn in steps required before the chain reaches a steady state is not some fixed number but rather depends on particular fit that you are running, though plotting the steps will help in determining the number of burn in steps that are necessary.

The Affine Invariant

While this procedure describes a typical Metropolis-Hastings MCMC sampler, the version applied in emcee also adds an affine invariant, predominantly for the sake of efficiency. The premise of this addition is to consider a set of walkers, each moving individually step by step. Their steps, however, are interconnected in that for each walker, the choice for the next proposed step depends on another randomly chosen walker.[3] This new proposed location of x_1 with x_0 as the other walker will be given by $x_0 + a(x_1 - x_0)$ where a is a random variable generated from a distribution chosen by the user. The acceptance of steps is done in a similar way to that already describted, though a more detailed description of this method can be found in [18].

Methods of Model Selection

In modelling, we need methods to compare models and choose those that we consider to be optimal. Especially with complex models like those used to fit our physical models, this can involve a large amount of parameter selection and a number of potential models. In order to differentiate these models, we chose to use two main metrics: the value of the maximum log likelihood and the Bayesian Inference Criterion (BIC).

The maximum log likelihood value was already described above, and the model with the largest value would be considered best by this model. While maximum log likelihood is a reasonable metric, there are a few cautions to consider with the method. First, recall that its value is meant for comparison and is only really useful when being compared relative to the value of other related model. Another caution, which is our main point of concern, is that this method does not control for model complexity. By this, we mean that by this metric, adding more parameters to our model will generally increase the maximum log likelihood.[4] The issue with this, however, is that it creates a risk of overfitting the data. By overfitting, we refer to a scenario where our model becomes too dependent on the specific data presented

[3] In practice, the walkers are actually divided into two groups where each move for one walker is determined based on a random walker from the other group. This is done so that the walkers in each group can take steps in parallel with the two groups alternating steps.

[4] It should not be hard to convince yourself of this fact. For instance, consider a simple power law. If we then added a cutoff, a third parameter, then this will either improve how well our model appears to match the data, or the cutoff will be placed at a high enough value to have practically no impact.

instead of modelling the overall trend that this data represents. Put simply, we want to find the simplest model to explain the data.

We therefore want to use a criterion that penalizes model complexity. To do so, we primarily implemented the BIC, which adjusts the log likelihood value, MLL to penalize model complexity. BIC is given as $BIC = -2MLL + log(n)p$ where MLL is the maximum log likelihood value, n is the the number of observations, and p is the number of parameters. As may be apparent by the formula, we ideally want a model with a low BIC value.[5]

Of course, there are other considerations to make in the course of model selection, though these criteria are useful to help in the process. In model selection, we should always be aware of our modelling goals as well as the context in which we are modelling. This includes instances like in Chapter 4 where we found that a model with slightly worse BIC seemed to better explain the data in the range that we were interested in and ensuring that our model parameters fall within a range that makes physical sense, for instance avoiding creating negative energies or negative magnetic field strengths.

[5]There are, of course, other criteria that can be used. One common one, which is closely related to BIC is the Alkaline Information Criterion (AIC), which is given by $AIC = -2MLL + 2p$, a similar metric to BIC with a smaller penalty on complexity. Like BIC, better models have lower values of AIC.

Academic Vita
Leah Hunt

Education

Bachelor of Science in Mathematics, Bachelor of Science in Statistics 2021 (expected)
with minors in Economics, IST for Math, and History
The Pennsylvania State University, Schreyer Honors College

Work Experience

LiveOnline SAT Teacher/Tutor - The Princeton Review 01/2018-present

- Engage students in online learning environment
- Analyze scoring trends of individual students to suggest methods for improvement

Research Experience

Honors Thesis Research – Penn State 01/2018-present

- Analyze high energy emissions of supernova remnants
- Combine data from multiple experiments to fit empirical and physically motivated models for energy emissions, particularly of the supernova remnant IC 443
- Presented at April 2019 and April 2020 American Physical Society general meetings

BOAST Project – Penn State Summer 2020 – Fall 2020

- Develop apps using shiny in R with the purpose of teaching concepts in statistics
- Modify existing code to improve code structure, fix bugs, and improve app functionality

Leadership and Activities

Math Club
Webmaster (04/2019-present) 08/2017-present

- Manage the club website
- Track club attendance
- Work with the other officers to organize the agenda for club meetings

Statistics Club
Webmaster (04/2020-present) 08/2019-present

- Manage the club website
- Work with the other officers to organize the agenda for club meetings

Schreyer Student Council

- Develop and execute service projects with the service committee 08/2017-present
- Work with the honors college to plan social activities, merchandise sales, and other events

Diaper Depot at Central
Volunteer Spring 2016-Winter 2020

- Welcome new families
- Help families through the registration process
- Wrote two support letters for grants to the program

Computer and Technical Skills

- Python, R, Java, C++